ALTERNATING OPTIMIZATION METHOD FOR ISOGEOMETRIC TOPOLOGY OPTIMIZATION WITH STRESS CONSTRAINTS*

Xiaoya Zhai

School of Mathematical Sciences, University of Science and Technology of China, Hefei 230071, China
Email: xiaoya93@mail.ustc.edu.cn

Abstract

Topology optimization (TO) has developed rapidly recently. However, topology optimization with stress constraints still faces many challenges due to its highly non-linear properties which will cause inefficient computation, iterative oscillation, and convergence guarantee problems. At the same time, isogeometric analysis (IGA) is accepted by more and more researchers, and it has become one important tool in the field of topology optimization because of its high fidelity. In this paper, we focus on topology optimization with stress constraints based on isogeometric analysis to improve computation efficiency and stability. A new hybrid solver combining the alternating direction method of multipliers and the method of moving asymptotes (ADMM-MMA) is proposed to solve this problem. We first generate an initial feasible point by alternating direction method of multipliers (ADMM) in virtue of the rapid initial descent property. After that, we adopt the method of moving asymptotes (MMA) to get the final results. Several benchmark examples are used to verify the proposed method, and the results show its feasibility and effectiveness.

Mathematics subject classification: 49J20, 65J15, 65N30.
Key words: Isogeometric topology optimization, Stress constraints, The ADMM-MMA solver.

1. Introduction

Topology optimization (TO) is a mathematical method that finds the optimal material layout by a given design domain under a set of loads, and boundary conditions [1]. It can be classified into two types according to the properties of different optimized objects, that are, topology optimization of continuum structures and discrete structures. Topology optimization of continuum structures is a hot topic nowadays. It can be applied to various fields, such as aerospace, bio-engineering, architectural design and so on.

Bendsoe and Kikuchi [2] first introduced the conception of the topology optimization of continuum structures and put forward a homogenization method that generated optimal topologies. Thereafter, a series of works came out. At present, there are many practical and effective numerical methods of topology optimization of continuum structures such as homogenization method [2], the solid isotropic material with penalization (SIMP) method [3, 4], the level set method [5], the moving morphable components (MMC) method [6, 7] and the moving morphable void (MMV) method [8, 9]. It is very difficult to solve topology optimization of continuum structures by the analytical method due to its nonlinearity. Most current methods adopt the numerical algorithm during calculation, which is based on finite element analysis (FEA). However, low-order shape functions often lead to numerical instabilities, slow convergence and

---

iterative oscillation. Moreover, the gap and barrier between geometric representation and finite element analysis (FEA) still exist. The isogeometric analysis (IGA) offers us the opportunity for integrating computer-aided design (CAD) and computer-aided engineering (CAE), which was proposed by Huges et al. [10]. Recently, isogeometric analysis has already been applied to the field of topology optimization, which is called isogeometric topology optimization (ITO) because of its higher accuracy than traditional FEA. Kim et al. [11] extended IGA to the topology optimization by trimming the spline. Kumar et al. [12] used B-spline elements to represent the density function for topology optimization. They applied the implicit boundary method to boundary conditions and loads. Finally, they made a comparison with traditional elements and the results indicated that B-spline elements naturally tend to suppress shape irregularities and stability. Hassani et al. [13] proposed an isogeometric approach to topology optimization by optimality criteria. The results are independent of the number of discrediting control points and checkerboard free. Qian [14] represented the density distribution by B-splines over a rectangular domain, and this representation is compact in storage and does not require neighboring element information. Lin et al. [15] developed a unified strategy to simultaneously insert inclusions or holes of regular shape as well as the material to affect optimal topologies of solids. Wang et al. [16] introduced isogeometric topology optimization for periodic lattice materials to improve computational accuracy and efficiency and get faster convergence.

In practical engineering applications, the optimization problem with stress constraints is very important so that we can not ignore it. In 1996, Yand and Chen [17] studied stress-based topology optimization. They summarized the major difficulties of solving this problem. The first one is numerous constraints because of the local quantity of stress. This property will result in a huge computational burden of both optimization and sensitivity analysis. The second one is highly nonlinear with design variables. Later, Bendsoe and Sigmund [18] added one challenging issue, that is, the stress singularity phenomenon. The stress singularity arises in the density-based optimization approaches due to the discontinuity of local stress constraints when topology design variables tend to the critical values. It may prevent optimization algorithms from finding the true optimal material distribution [19]. We summarize three difficulties in topology optimization with stress constraints, which are as follows:

- Numerous stress constraints due to the local quantity of stress;

- Highly nonlinear properties;

- Stress singularity issues;

Later, researchers put forward different optimization models to solve the above three problems. Firstly, to avoid the huge computational burden created by local quality, the local stress constraints are often replaced with some stress aggregation formulation such as the P-norm function [20] and the Kreisselmeier Steinhauser (K-S) function [21]. However, instability will occur in the calculation process through the approximation of these two methods. The key is to make a trade-off between computational accuracy and efficiency. There are some works to illustrate this problem including the normalized P-norm measure approach [22], the improved penalty functional approach [23], the shape equilibrium constraint strategy [24], the global stress measure method [25] and several recently developed numerical techniques [26]. Secondly, stress constraints are highly nonlinear. To remedy this situation, Francavilla et al. [27] presented the optimization of shape to minimize stress concentration. Despite this, Walter [28] detailed introduced the factors that lead to stress concentration. Thirdly, researchers put forward some

methods such as the epsilon-relaxation method [29], the *qp* relaxation method [30] to avoid stress singularity. Although there are many ways to solve stress-based topology optimization, it is still an open problem to establish new stress constraint formulations that make problems more efficient and convergence. Liu et al. [31] solved the IGA-SIMP model with global stress constraint and the results showed it avoided the obvious zigzag boundaries. They choose a stability transformation method (STM)-based stabilization scheme in the optimization process. In this paper, we use the IGA-SIMP model to solve the topology optimization with stress constraints and choose a p-norm scheme to approximate the maximum stress and an STM-stable scheme to ensure iteration stability.

Numerical methods of topology optimization can be divided into three types: the criterion algorithm, the mathematical programming algorithm, and the intelligent algorithm [32]. The criterion algorithm is also called the optimal criterion (OC) algorithm such as the Lagrange multiplier algorithm with KKT conditions. The evolutionary structural optimization (ESO) method [33] is also the typical criterion method. The mathematical programming algorithm mainly includes sequential quadratic programming algorithm (SQP) [34], penalty and augmented Lagrangian algorithm, the primal-dual interior point method [35] and so on. This mathematical programming can also be used in topology optimization. Out of all of these methods, Svanberg put forward the method of moving asymptotes (MMA) [36] in 1987, later he promoted its convergence and came up with its globally convergent counterpart (GCMMA) [37] in 2002. Susana and Mathias [38] made a comparison of these methods in some iterations, and parameters when applied to various finite elements based topology optimization problems. The intelligent algorithm is also used commonly in topology optimization including genetic algorithm (GA) [39], simulated annealing (SA) algorithm [40], the particle swarm method [41] and so on. One of the advantages of these algorithms is to omit the calculation of sensitivity analysis. But when the scale of the problem is larger, optimization efficiency is decreased significantly. In this paper, we mix the two algorithms which are **A**lternating **D**irection **M**ethod of **M**ultipliersto (ADMM) and MMA to improve computational efficiency.

The structure of this paper is organized as follows. In Section 2, we briefly review some basic definitions of **N**on**U**niform **R**ation **B**-**S**pline (NURBS) and representation. In Section 3, we describe the ADMM-MMA solver for topology optimization problems with global stress constraints. In Section 4, experimental results are demonstrated and comparisons are made between various methods on several factors (optimization time, number of iterations, and the objective values). After that, we make a discussion on the alternating optimization method. We conclude the paper with a summary in the last section and look to future work.

2. Preliminaries

In this section, we present the definition and general properties of **N**on**U**niform **R**ational **B**-**S**pline (NURBS) basis functions and surface representations. Model formulation of topology optimization based on isogeometric analysis is also given.

2.1. NURBS functions

2.1.1. Definition and Properties of B-Spline Basis Functions

Given a *knot vector* $\boldsymbol{T} = \{t_0, t_1, \cdots, t_{n+p}\}$ ($\forall i, t_i \leq t_{i+p}$), the t_i are called knots. The associated B-spline functions are recursively defined by
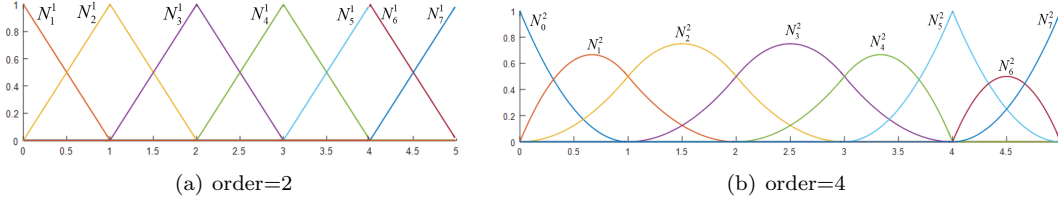
(a) order=2   (b) order=4

Fig. 2.1. (a) The nonzero first-degree basis function, $\boldsymbol{T} = \{0,0,0,1,2,3,4,4,5,5,5\}$; (b) The nonzero second-degree basis functions, $\boldsymbol{T} = \{0,0,0,1,2,3,4,4,5,5,5\}$.

$$N_i^p(t) = \frac{t - t_i}{t_{i+p-1} - t_i} N_i^{p-1}(t) + \frac{t_{i+p} - t}{t_{i+p} - t_{i+1}} N_{i+1}^{p-1}(t),$$

where

$$N_i^1(t) = \begin{cases} 1, & t_i \leq t \leq t_{i+1}; \\ 0, & \text{else}; \end{cases}$$

where n is the number of basis functions, p is the polynomial order (degree $p-1$). If the knots are distributed equally, it is called uniform knots span, otherwise called non-uniform knots span.

2.1.2. Definition and Properties of NURBS surfaces

Given a *knot vector* $\boldsymbol{S} = \{s_0, s_1, \cdots, s_{n+p}\}$, $(\forall i, s_i \leq s_{i+p})$ and a *knot vector* $\boldsymbol{T} = \{t_0, t_1, \cdots, t_{m+q}\}$, $(\forall j, t_j \leq t_{j+q})$, therein, p and q are the order in the s and t directions, respectively. A NURBS surface is represented as follows

$$R(s,t) = \frac{\sum_{i=0}^{n} \sum_{j=0}^{m} N_i^p(s) N_j^q(t) w_{i,j} P_{i,j}}{\sum_{i=0}^{n} \sum_{j=0}^{m} N_i^p(s) N_j^q(t) w_{i,j}}, \quad 0 \leq s, t \leq 1. \tag{2.1}$$

$\{P_{i,j}\}_{i=0,j=0}^{n,m}$ forms a bidirectional control net, $\{w_{i,j}\}_{i=0,j=0}^{n,m}$ is weight parameter and the $N_i^p(s)$ and $N_j^p(t)$ are the NURBS basis which are defined on *knots vector* $\boldsymbol{S}$ and $\boldsymbol{T}$. In Fig. 2.2, we draw the tensor product surface of the basis function of s and t directions. Further, we define $R_{i,j}^{p,q}(s,t)$ as follows

$$R_{i,j}^{p,q}(s,t) = \frac{N_i^p(s) N_j^q(t) w_{i,j}}{\sum_{i=0}^{n} \sum_{j=0}^{m} N_i^p(s) N_j^q(t) w_{i,j}}.$$

So the Eq. (2.1) can be written as

$$R(s,t) = \sum_{i=0}^{n} \sum_{j=0}^{m} R_{i,j}^{p,q}(s,t) P_{i,j}.$$

The properties of NURBS surfaces are also briefly listed as follows:

(1) Local support. $R_{i,j}^{p,q}(s,t)$ is a step function, equal to zero everywhere except on $s \in [s_i, s_{i+p})$ and $t \in [t_j, t_{j+q})$.

(2) Non-negativity: $R_{i,j}^{p,q}(s,t) \geq 0$, $\forall i, j, s, t$.

(3) Partition of unity: $\sum_{i=0}^{n} \sum_{j=0}^{m} R_{i,j}^{p,q}(s,t) = 1$ for all $(s,t) \in [0,1] \times [0,1]$.

(a) parameter space   (b) NURBS basis   (c) NURBS surface
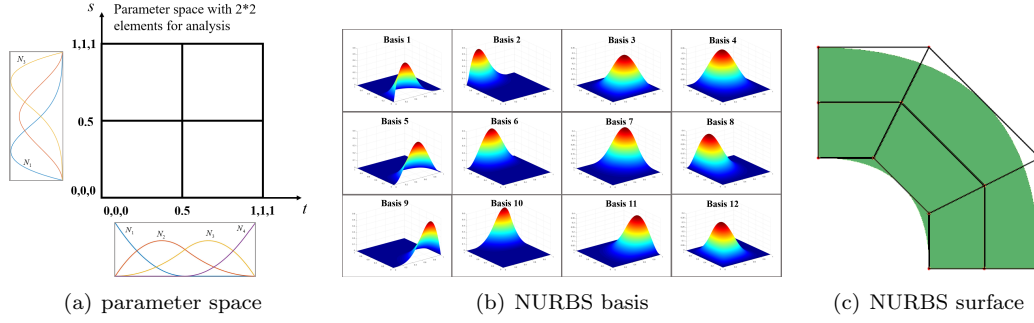
Fig. 2.2. Given $S = [0, 0, 0, 0.5, 1, 1, 1]$, $T = [0, 0, 0, 0.5, 1, 1, 1]$.(a) Parameter space. (b) NURBS basis. (c) NURBS surface.

(4) In any given rectangle of the form $[s_i, s_{i+1}) \times [t_j, t_{j+1})$, at most $(p + 1) \times (q + 1)$ basis functions are nonzero.

2.2. Representation by IGA

We briefly recall the model formulation of static equilibrium analysis, for elaboration, refer [42]. After that, we detailed describe the isogeometric analysis representation.

In structural analysis, given a design region Ω, the external force $\boldsymbol{f}$ and boundary conditions BC, the material distribution $\boldsymbol{\rho}$ under the maximum stress constraints $\max(\boldsymbol{\sigma})$ (less than the yield force $\boldsymbol{\sigma_0}$) is optimized. It should emphasize that $\boldsymbol{\sigma_0}$ is constant for a given material. In response to such problems, it is usually divided into three parts, region subdivision, element analysis and model solution. In this subsection, we focus on element analysis. It is noted that elastic mechanics study the elastic deformation phase of the elastomer, after the removal of external forces, the elastomer can be restored to its original state. So all equations are under the assumption of small deformations.

Here, $\boldsymbol{\varepsilon}$ and $\boldsymbol{\sigma}$ are denoted as the strain tensor and the stress tensor. The relevant calculation of the equilibrium equation is as follows

$$K\boldsymbol{u} = \boldsymbol{f}, \tag{2.2}$$

$$\boldsymbol{\varepsilon} = B\boldsymbol{u}, \quad \boldsymbol{\sigma} = D \cdot \boldsymbol{\varepsilon} = DB\boldsymbol{u},$$

where K is the global stiffness matrix which is composed of element stiffness matrices as

$$K = \sum K_e, \quad K_e = \int_{\Omega_e} B^T DB d\Omega_e.$$

Eq. (2.2) is called equilibrium equation. Matrix B is a strain matrix that only depends on the shape of the element. When elements are generated and then the node coordinates are determined, the matrix B is a constant matrix. The matrix D is called the elastic matrix (elastic tensor). It is a constant matrix that is associated with the modulus of elasticity E and Poisson's ratio μ. The modulus of elasticity E is density-dependent. Some researchers [42] suggests they have a power-law relationship, that is, $E = \boldsymbol{\rho}^k E_0$ (k=3). The elastic matrix D

(a) Real design domain   (b) Parameter domain   (c) Integral domain
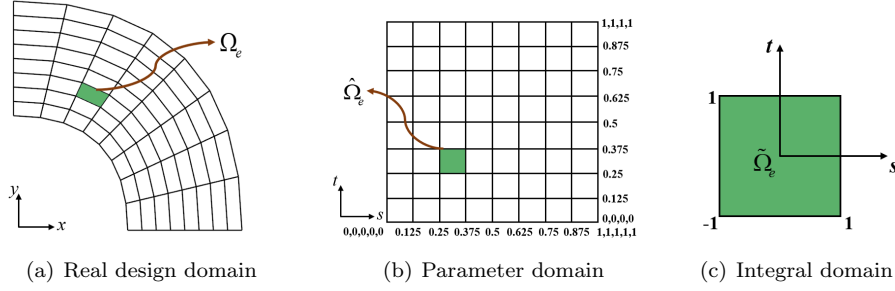
Fig. 2.3. (a) The real design domain; (b) The parameter domain with $T = \{0,0,0,0,0,0.125, 0.25, 0.375, 0.5,0.625,0.75,0.875,1,1,1,1,1\}$ and $S = \{0,0,0,0,0,0.125,0.25,0.375,0.5,0.625,0.75,0.875,1,1,1,1,1\}$. (c) The integral domain.

can be represented as

$$D = \frac{E}{1-\mu^2}\begin{bmatrix} 1 & \mu & 0 \\ \mu & 1 & 0 \\ 0 & 0 & \frac{1-\mu}{2} \end{bmatrix} = \frac{\boldsymbol{\rho}^k \cdot E_0}{1-\mu^2}\begin{bmatrix} 1 & \mu & 0 \\ \mu & 1 & 0 \\ 0 & 0 & \frac{1-\mu}{2} \end{bmatrix} = \boldsymbol{\rho}^k D_0.$$

The von Mises yield criterion stipulates that if the von Mises stress of a material under load is equal to or greater than the yield limit of the same material under simple tensile force (which is easily determined experimentally), then the material will yield. Von Mises stress σ^{vm} can be calculated by $\boldsymbol{\sigma}$ through transfer matrix $\bar{V}$:

$$\sigma^{vm} = (\boldsymbol{\sigma}^T \bar{V} \boldsymbol{\sigma})^{\frac{1}{2}}, \qquad \bar{V} = \begin{bmatrix} 1 & -\frac{1}{2} & 0 \\ -\frac{1}{2} & 1 & 0 \\ 0 & 0 & 3 \end{bmatrix}.$$

Based on the concept of isogeometric analysis, NURBS are employed not only as a geometry representation, but also a discretization tool for structural analysis. At first, we define Ω as the physical domain and $\hat{\Omega}$ as the parameter domain. In this paper, we perform k-refinement to obtain a subdivision, and then we can get many small elements $\hat{\Omega}_e$. Next, we take the NURBS basis functions as shape functions during the processing of analysis. The displacement $\boldsymbol{u}$ (the density $\boldsymbol{\rho}$) of any points is the combination of displacements at the control points u_{ij} (ρ_{ij}). It can be described as follows

$$u(s,t) = \sum_{i=0}^{n}\sum_{j=0}^{m} R_{i,j}^{p,q}(s,t)u_{i,j} \;\; \Rightarrow \;\; u_e = \sum_{i=0}^{n}\sum_{j=0}^{m} R_{i,j}^{p,q}(s_e^c,t_e^c)u_{i,j}, \qquad (2.3)$$

$$\rho(s,t) = \sum_{i=0}^{n}\sum_{j=0}^{m} R_{i,j}^{p,q}(s,t)\rho_{i,j} \;\; \Rightarrow \;\; \rho_e = \sum_{i=0}^{n}\sum_{j=0}^{m} R_{i,j}^{p,q}(s_e^c,t_e^c)\rho_{i,j}, \qquad (2.4)$$

where $u_{i,j}$ and $\rho_{i,j}$ are the displacement and density control coefficients. For efficient calculation, the displacement function and the density function in the element centroid are chosen, the representation can be shown on the right side of Eqs. (2.3)–(2.4).

Similarly, if we want to calculate any variables (such as stress σ, strains ε) at any point in the physical domain Ω, it can be obtained by weighting NURBS basis. It's important to note that all integrals are converted to Gauss integrals, defined at $[0,1] \times [0,1]$.

3. Methods

3.1. Formulation of optimization problem

In this paper, we take a design domain, external forces, and boundary conditions as the inputs and structural volume as the objective function. The maximum stress is adopted as the constraint. So the topology optimization problem can be formulated mathematically as follows,

$$(\mathcal{P}) \quad Find \quad \boldsymbol{\rho} = (\rho_{1,1}, \rho_{1,2} \ldots \rho_{1,n}, \ldots, \rho_{m,1}, \rho_{m,2}, \ldots, \rho_{m,n})$$

$$\min \quad V(\rho_{i,j}) = \sum_{e=1}^{N_e} \rho_e v_e \tag{3.1}$$

$$\text{s.t. } K\boldsymbol{u} = \boldsymbol{f}, \tag{3.2}$$

$$\max(\boldsymbol{\sigma}^{vM}) \leq \sigma_0, \tag{3.3}$$

$$0 < \rho_{\min} \leq \rho_{i,j} \leq 1, \tag{3.4}$$

where Eq. (3.1) represents the structural volume. $\rho_{i,j}$ $(i = 1, \ldots, n; j = 1, \ldots, m;)$ is the design variables. ρ_e $(e = 1, \ldots, N_e)$ is the density of the e-th element. It is interpolated by NURBS basis. The relationship between $\rho_{i,j}$ and ρ_e can be referred to Eq. (2.4). v_e $(e = 1, \ldots, N_e)$ is the volume of the e-th element and N_e is the number of elements. K represents the stiffness matrix. $\boldsymbol{u}$ denotes the displacement control coefficients. $\boldsymbol{f}$ is external forces. Constraint (3.3) is the stress constraints. $\boldsymbol{\sigma}^{VM} = \{\sigma_1^{VM}, \sigma_2^{VM}, \cdots, \sigma_{N_a}^{VM}\}$, N_a is the number of Gauss points. We calculate the stress at the Gauss point P_a $(a = 1, \ldots, N_a)$. In this paper, we adopt P-norm scheme to approximate the maximum stress $\max(\sigma_a^{vM})$. σ_0 implies yield stress of materials. We refer to the paper [31] and use the STM stabilization scheme to avoid iterative oscillation. The P-norm stress and relaxation functions are stated as follows:

$$\max(\boldsymbol{\sigma}^{vM}) \approx \boldsymbol{\sigma}^{Pnorm} = \Big(\sum_{a=1}^{N_a} (\rho_a^s \sigma_a^{vM})^{Pnorm} \Big)^{\frac{1}{Pnorm}},$$

where $Pnorm = 16$ and $s = \frac{1}{2}$. Bound constraints (3.4) are discretized the density from two values of 0-1 into a continuous variation between 0 and 1. $\rho_{\min}$ is a small positive number, in this paper, we set $\rho_{\min} = 0.001$ to avoid singularity in stiffness matrix.

3.2. ADMM-MMA solver

The formulation stated in Section 3.1 is a nonconvex optimization problem. We can find that the objective function is linear, and stress constraints are highly nonlinear. In this section, a new optimization method is proposed for isogeometric topology optimization with stress constraints. We first generate an initial feasible point by alternating direction method of multipliers (ADMM) due to its property of rapid initial descent. After that, we adopt the method of moving asymptotes (MMA) introduced in paper [36] to get the final results.

3.2.1. Determine an initial feasible point by ADMM

We first introduce the details of getting an initial feasible point by ADMM. We transfer the original problem ($\mathcal{P}$) into the followed formulation by converting mandatory constraints into soft constraints through penalty functions $\mu(\boldsymbol{\sigma}^{VM} - \max(\sigma_a^{VM}))$ and adding Lagrange multiplier
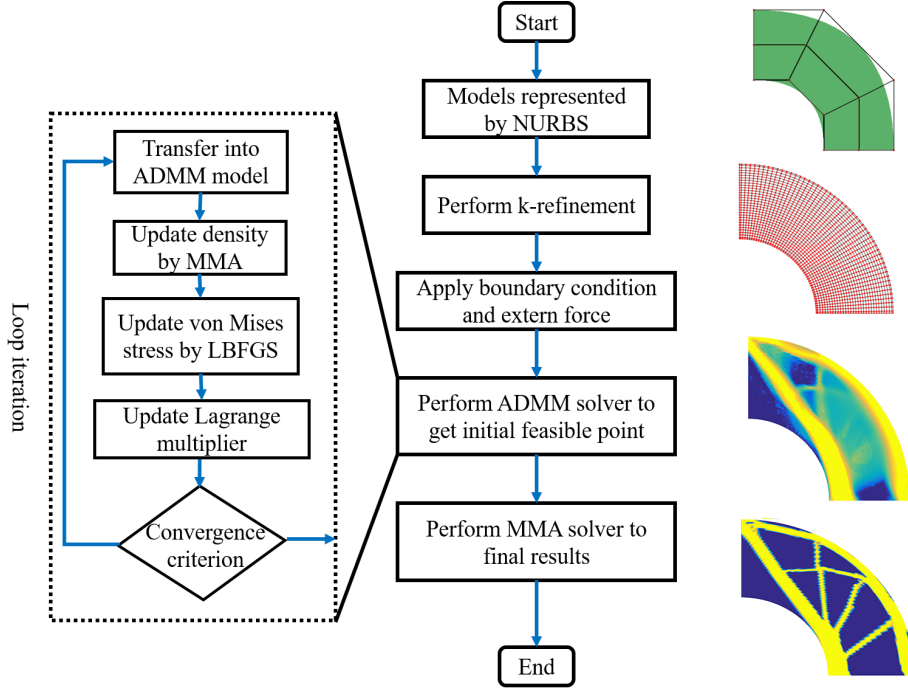
Fig. 3.1. The pipeline of our algorithm.

$\boldsymbol{\lambda}$ and parameter η:

$$L(\boldsymbol{\rho}, \boldsymbol{\sigma}^{VM}, \boldsymbol{\lambda}) = \sum \rho_e v_e + \mu(\sigma_0 - \max(\boldsymbol{\sigma}^{VM})) + \boldsymbol{\lambda}^T(\boldsymbol{\sigma}^{VM} - g(\boldsymbol{\rho}))$$
$$+ \frac{\eta}{2}\|\boldsymbol{\sigma}^{VM} - g(\boldsymbol{\rho})\|^2, \tag{3.5}$$

where ρ_e and $\rho_{i,j}$ $(i = 1, \ldots, n; j = 1, \ldots, m)$ are the same meaning as previous definition which is bounded by constraints $\rho_{\min} \le \rho_{i,j} \le 1$. The general requirements of penalty function $\mu(x)$ are as follows:

$$\mu(x) = \begin{cases} \infty, & x > 0; \\ 0, & x \le 0; \end{cases}$$

$\mu(x) = c_1 \cdot x^{c_2}$ is taken as smooth penalty function to ensure the differentiability. Here, we use $g(\boldsymbol{\rho})$ to approximate von Mises stress $\boldsymbol{\sigma}^{VM}$. The formulation is as follows:

$$g(\rho_{i,j}) = (D(\rho_{i,j}) \cdot B_a \cdot D(\rho_{i,j})^T V D(\rho_{i,j}) \cdot B_a \cdot D(\rho_{i,j})^T)^T, \tag{3.6}$$

where $D(\boldsymbol{\rho}) = \boldsymbol{\rho}^k D_0$. D_0 is the elastic matrix. B_a is an elastic displacement matrix on an element. In this paper, we set $\lambda_k = 0.001$ $(k = 1, \cdots, N_a)$, $\eta = 0.001$ and $c_1 = 100000, c_2 = 5$.

In Eq. (3.5), we regard density $\rho_{i,j}$ and von Mises stress $\boldsymbol{\sigma}^{VM}$ as two independent variables for optimization respectively to obtain the final results. These two design variables are connected by the Eq. (3.6). We transfer the formulation into two-block optimization processes. The first block takes $\boldsymbol{\rho}$ as design variables, while $\boldsymbol{\sigma}^{VM}$ is the design variables in the second block.

Finally, we update the parameter $\boldsymbol{\lambda}$. The optimization formulations are stated as follows:

$$L(\boldsymbol{\rho}^{[k]}) = \sum \boldsymbol{\rho}_e^{[k]} v_e + \boldsymbol{\lambda}^T((\boldsymbol{\sigma}^{VM})^{[k]} - g(\boldsymbol{\rho}^{[k]})) + \frac{\eta}{2}\|(\boldsymbol{\sigma}^{VM})^{[k]} - g(\boldsymbol{\rho}^{[k]})\|^2, \tag{3.7}$$

$$L((\boldsymbol{\sigma}^{VM})^{[k]}) = \mu(\sigma_0 - \max((\boldsymbol{\sigma}^{VM})^{[k]})) + \boldsymbol{\lambda}^T((\boldsymbol{\sigma}^{VM})^{[k]} - g(\boldsymbol{\rho}^{[k+1]}))$$

$$+ \frac{\eta}{2}\|(\boldsymbol{\sigma}^{VM})^{[k]} - g(\boldsymbol{\rho}^{[k+1]})\|^2, \tag{3.8}$$

$$\boldsymbol{\lambda}^{[k+1]} = \boldsymbol{\lambda}^{[k]} + \eta((\boldsymbol{\sigma}^{VM})^{[k+1]} - g(\boldsymbol{\rho}^{[k+1]})). \tag{3.9}$$

Under the 2-block framework, the basic form of our ADMM algorithm is:

$$\boldsymbol{\rho}^{[k+1]} = \arg\min L(\boldsymbol{\rho}^{[k]}, (\boldsymbol{\sigma}^{vM})^{[k]}, \boldsymbol{\lambda}^{[k]}), \tag{3.10}$$

$$(\boldsymbol{\sigma}^{vM})^{[k+1]} = \arg\min L(\boldsymbol{\rho}^{[k+1]}, (\boldsymbol{\sigma}^{VM})^{[k]}, \boldsymbol{\lambda}^{[k]}), \tag{3.11}$$

$$\boldsymbol{\lambda}^{[k+1]} = \boldsymbol{\lambda}^{[k]} + \eta(\boldsymbol{\sigma}^{[k+1]} - g(\boldsymbol{\rho}^{[k+1]})). \tag{3.12}$$

Feasible points can be obtained by alternately optimizing density $\boldsymbol{\rho}$ and von Mises stress $\boldsymbol{\sigma}$ in the initial iterations. And then, the Method of Moving Asymptotes (MMA) [36] is adopted to get the final results. From the experimental results, it shows the initial stage of the iteration process decreases rapidly. It should be noted that due to the highly nonlinear properties of the problem, oscillation cannot be avoided in the process of iteration. The calculation process of our algorithm is shown in Fig. 3.1.

3.3. Sensitivity analysis

We introduce the sensitivity formulation in the ADMM method. The sensitivity analysis of the original problem can be transformed into the sensitivity analysis of two block problems. In Eq. (3.7), we fix the variable $\boldsymbol{\sigma}^{VM}$, $\boldsymbol{\lambda}$ and iterated the optimal density $\boldsymbol{\rho}$ through the current loop. To get sensitivity of Eq. (3.7), we need to calculate $\frac{\partial V}{\partial \rho_{ij}}$ and $\frac{\partial g(\boldsymbol{\rho})}{\partial \rho_{ij}}$. In Eq. (3.8), we fix the variable iterated from the first block problem $\boldsymbol{\rho}$, $\max(\boldsymbol{\sigma}^{VM})$, $g(\boldsymbol{\rho})$ and iterated the optimal von Mises $\boldsymbol{\sigma}^{VM}$ through the current loop.

The sensitivity of the first block problem. It mainly concludes $\frac{\partial V}{\partial \rho_{ij}}$ and $\frac{\partial g(\boldsymbol{\rho})}{\partial \rho_{ij}}$. The derivative of material volume with respect to density ρ_{ij} reads

$$\frac{\partial V}{\partial \rho_{ij}} = \frac{\partial \sum_{e=1}^{N_e} \rho_e v_e}{\partial \rho_{ij}} = \sum_{e=1}^{N_e} \frac{\partial \rho_e}{\partial \rho_{ij}} \cdot v_e,$$

$$\frac{\partial \rho_e v_e}{\partial \rho_{ij}} = R_{ij}^{pq}(\xi_e^c, \eta_e^c) = R_{ij},$$

$$\frac{\partial V}{\partial \rho_{ij}} = \sum_{e=1}^{N_e} R_{ij} \cdot v_e.$$

To calculate the derivative of $g(\boldsymbol{\rho})$ with respect to density ρ_{ij}, we first analysis $g(\boldsymbol{\rho})$. $g(\boldsymbol{\rho})$ is a vector and ρ_{ij} $(i \in [0, N_x], j \in [0, N_y])$ is also a vector. $g(\boldsymbol{\rho}) = (g_1(\rho), g_2(\rho), \cdots, g_{N_a}(\rho))$,

N_a is a number of Gauss points. So $\frac{\partial g(\boldsymbol{\rho})}{\partial \boldsymbol{\rho}}$ is a matrix with N_a rows and m cols, that is

$$
\frac{\partial g(\boldsymbol{\rho})}{\partial \boldsymbol{\rho}} = \begin{bmatrix} \dfrac{\partial g_1(\rho)}{\partial \rho_1} & \dfrac{\partial g_1(\rho)}{\partial \rho_2} & \cdots & \dfrac{\partial g_1(\rho)}{\partial \rho_{N_x \times N_y}} \\ \vdots & \vdots & \vdots & \vdots \\ \dfrac{\partial g_{N_a}(\rho)}{\partial \rho_1} & \dfrac{\partial g_{N_a}(\rho)}{\partial \rho_2} & \cdots & \dfrac{\partial g_{N_a}(\rho)}{\partial \rho_{N_x \times N_y}} \end{bmatrix},
$$

where N_x and N_y are the number of elements divided in u and v directions.

Let us choose an element $\frac{\partial g_a}{\partial \rho_{ij}}$ of the matrix $\frac{\partial g(\boldsymbol{\rho})}{\partial \boldsymbol{\rho}}$. Further, the derivative of the function $g(\boldsymbol{\rho})$ with respect to the design variable ρ_{ij} in terms of chain rule shows as follows:

$$
\frac{\partial g_a}{\partial \rho_{ij}} = \frac{\partial g_a}{\partial \boldsymbol{\sigma}_a} \cdot \frac{\partial \boldsymbol{\sigma}_a}{\partial \rho_{ij}}.
$$

As for the term A, we give the formulation of the von Mises stress. It is a combination of three variables $\sigma_x, \sigma_y, \sigma_{xy}$.

$$
\sigma^{VM} = \left(\frac{(\sigma_x - \sigma_y)^2}{2} + \frac{\sigma_x}{2} + \frac{\sigma_y^2}{2} + 3\tau_{xy}^2 \right)^{\frac{1}{2}}.
$$

So the derivative of $g(\boldsymbol{\rho})$ with respect to density ρ_{ij} is $\frac{\partial g(\boldsymbol{\rho})}{\partial \boldsymbol{\sigma}_a} = (\frac{\partial g(\boldsymbol{\rho})}{\partial \sigma_x}, \frac{\partial g(\boldsymbol{\rho})}{\partial \sigma_y}, \frac{\partial g(\boldsymbol{\rho})}{\partial \sigma_{xy}})$. Moreover,

$$
\frac{\partial \boldsymbol{\sigma}^{VM}}{\partial \sigma_x} = \frac{1}{2\boldsymbol{\sigma}^{VM}}(2\sigma_x - \sigma_y),
$$

$$
\frac{\partial \boldsymbol{\sigma}^{VM}}{\partial \sigma_y} = \frac{1}{2\boldsymbol{\sigma}^{VM}}(2\sigma_y - \sigma_x),
$$

$$
\frac{\partial \boldsymbol{\sigma}^{VM}}{\partial \tau_{xy}} = \frac{1}{3\tau^{xy}}(\boldsymbol{\sigma}^{VM}).
$$

The derivative of $\boldsymbol{\sigma}_a$ with respect to density ρ_{ij}, that is

$$
\frac{\partial \boldsymbol{\sigma}_a}{\partial \rho_{ij}} = \frac{\partial \rho_e^k}{\partial \rho_{ij}} D_0 B_a u_e + \rho_e^k D_0 B_a \frac{\partial u_e}{\partial \rho_{ij}} = k\rho_e^{k-1} D_0 B_a u_e + \rho_e^k D_0 B_a \frac{\partial u_e}{\partial \rho_{ij}}.
$$

To simplify, we can get the following formula:

$$
\frac{\partial \boldsymbol{\sigma}_a}{\partial \rho_{ij}} = k\rho_e^{k-1} D_0 B_a u_e - \rho_e^k D_0 B_a (-K_e^{-1}) \frac{\partial K_e}{\partial \rho_{ij}} u_e.
$$

Here, we adopt the adjoint method in the sensitivity analysis.

The sensitivity of the second block problem. In this part, we fix $g(\boldsymbol{\rho}^{k+1})$ and $\max(\boldsymbol{\sigma}^{VM})$. Compared to the first part, the part of sensitivity analysis is simpler. So the derivative of $L(\boldsymbol{\sigma}^{VM})$ with respect to density $\boldsymbol{\sigma}$ reads

$$
\begin{aligned}
\frac{\partial L(\boldsymbol{\sigma}^{VM})}{\partial \boldsymbol{\sigma}^{VM}} &= \frac{\partial \mu(\boldsymbol{\sigma}^{VM} - \max(\boldsymbol{\sigma}^{VM}))}{\partial \boldsymbol{\sigma}^{VM}} + \boldsymbol{\lambda}^T + \eta(\boldsymbol{\sigma}^{VM} - g(\boldsymbol{\rho})), \\
&= c_1 \cdot c_2 \cdot (\boldsymbol{\sigma}^{VM} - \max(\boldsymbol{\sigma}^{VM}))^{c_2 - 1} + \boldsymbol{\lambda}^T + \eta(\boldsymbol{\sigma}^{VM} - g(\boldsymbol{\rho})).
\end{aligned}
$$

4. Numerical Examples

In this section, we present several examples of stress-related topology optimization obtained with the proposed algorithm and implementation. We refer to current algorithms based on the SIMP model such as MMA, and GCMMA algorithms. We use five factors to evaluate the performance of the proposed algorithm, and they are volume ratio(V/V_0), optimization time(t), number of iterations(N_{iter}), stress distribution, and convergence stability. In addition, in the color map of stress distribution, the redder the region, the larger the von Mises stress value is, and vice versa. The parameters and symbols are shown in Table 4.1. All the algorithms are implemented in MATLAB 2015b and measured on an Inter(R) $Core^{TM}$ i7-8550U CPU @1.80GHz with 16GB RAM.

Table 4.1: Parameters used in the numerical experiments.

Parameter	Description	Value
E	Young's modulus	$210\ GPa$
ν	Poisson's ratio	0.3
σ_0	The maximum yield stress	$358\ GPa$
Dr/DR	The inner/outer radius of the quarter annulus	$100/200\ mm$
DH/DW	The height/width of the model	$100/100\ mm$
Dh/Dw	The height/width of the short edge of L-shape model	$40/40\ mm$
f	The external force	$2000\ N$
p	SIMP penalization parameter	3
$maxiter$	Maximum number of iterations	1000
$Pnorm$	The parameter of P-norm stress function	16
N_{ele}	The number of elements	$10^3 - 10^4$
N_{iter}	The number of iterative steps	1000
$Pnorm$	The parameter of P-norm stress function	16

4.1. Quarter annulus structure design

First of all, the quarter annulus with stress-related topology optimization are solved to demonstrate the effectiveness of the proposed approach. All relevant geometry data as well as boundary conditions are introduced in Fig. 4.1(a). A vertical concentrated load is imposed in the upper-left corner of the model, and we fix the bottom of the model.
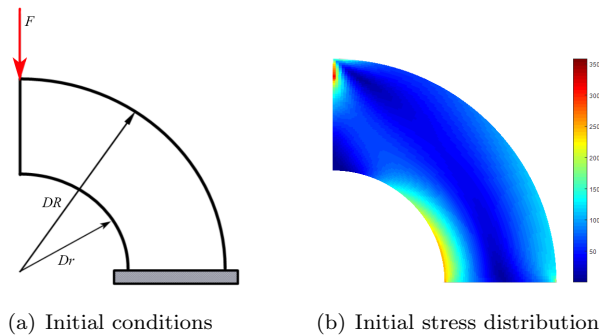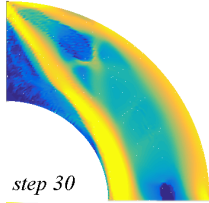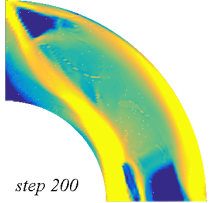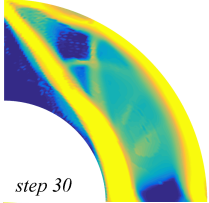

(a) Initial conditions   (b) Initial stress distribution
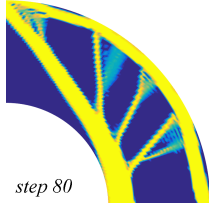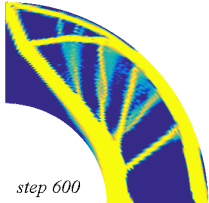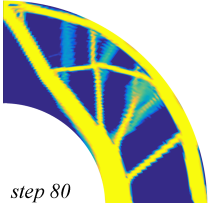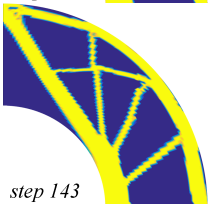
Fig. 4.1. Quarter annulus structure examples.

We test the effectiveness of our method compared with MMA and GCMMA under the girds 100×60. Table 4.2 lists the number of elements (N_{ele}), some intermediate iterative topologies

Table 4.2: Comparison of the topology optimization process among Quarter annulus examples with MMA, GCMMA, and ADMM-MMA.

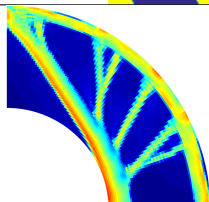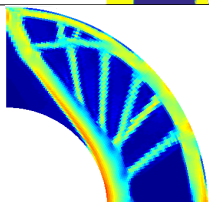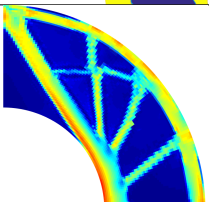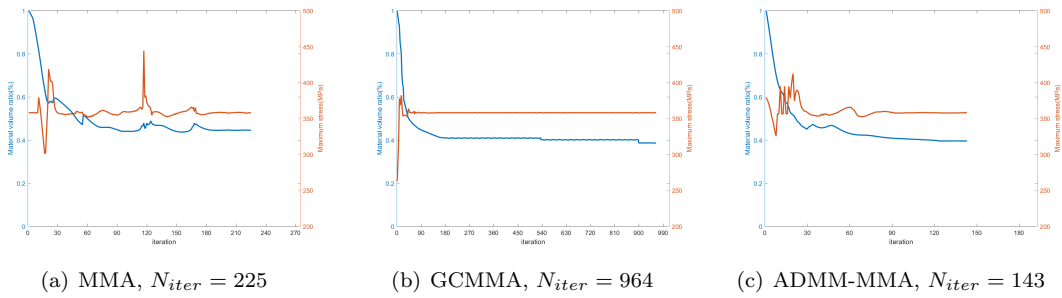| Methods	MMA	GCMMA	ADMM-MMA
N_{ele}	100×60	100×60	100×60
Intermediate topologies	step 30 / step 80 / step 225	step 200 / step 600 / step 965	step 30 / step 80 / step 143
Stress distribution			
N_{iter}	225	964	143
V/V_0	44.50%	38.58%	39.55%
$t(s)$	7137	32113	4856

(a) MMA, $N_{iter} = 225$ (b) GCMMA, $N_{iter} = 964$ (c) ADMM-MMA, $N_{iter} = 143$

Fig. 4.2. The convergence curve of three algorithms on the quarter annulus. The left horizontal axis represents the ratio of volume(V/V_0), the right horizontal axis represents the maximum von Mises($\max(\sigma)$) and the vertical axis represents iteration numbers.

and final optimal topology, final stress distribution, number of iterative steps (N_{iter}), volume ratio (V/V_0) and optimal time (t). On the one hand, our method can achieve acceptable designs. On the other hand, it is superior to MMA in these factors. It is also better than GCMMA in the

effectiveness of the algorithm. Generally, we use the number of iteration steps and optimization time to measure the rate of convergence. According to the comparison of total iteration steps and the column named Intermediate topologies among the three methods, it is clearly shown that the convergence using ADMM-MMA is faster than using the other two methods. Our algorithm takes the least time. It saves 32% time than MMA and 85% than GCMMA. From the colormap of stress distribution, our algorithm further reduces stress concentration. Apart from this, in the aspect of the objective function, our method is 4.95% less than MMA and 0.97% more than GCMMA.

Next, we analyze the convergence of solving isogeometric topology optimization with stress constraints by three algorithms. Fig. 4.2 shows the convergence plots for the Quarter annulus structure, where the left horizontal axis represents the ratio of volume (V/V_0), the right horizontal axis represents the maximum von Mises ($\max(\sigma)$) and the vertical axis represents iteration numbers. As can be seen from the figure, iteration oscillation occurs in MMA. Although GCMMA iterates smoothly, its convergence is slow. Our algorithm guarantees smooth iteration and fast convergence.

4.2. L-shaped beam design

The classical L-shape beam example for stress-related topology optimization is tested in this subsection. We fix the upper boundary and apply a downward force on the right side, shown in Fig. 4.3(a). In Fig. 4.3(b), serious stress concentration occurs near the corner marked by the red circle.

(a) Initial conditions   (b) Initial stress distribution
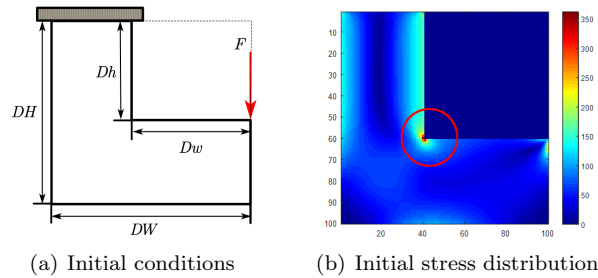
Fig. 4.3. L-shaped beam structure example.

We test three algorithms on L-shape structure and statistic number of iterations(N_{iter}), volume ratio(V/V_0) and optimization time(t) in Table 4.3. The operation time for every iteration is approximately 45.65s, 199.80s and 38.71s. The optimal topology can be obtained within 209, 311, and 178 iterations, respectively. From the objective function, our method is 3.43% less than MMA and 0.19% less than GCMMA. Our algorithm takes the least time. It saves 27.78% time than MMA and 88.90% than GCMMA.

Table 4.3: Comparison results on L-shaped beam structure with MMA, GCMMA and ADMM-MMA.

Methods	MMA	GCMMA	ADMM-MMA
N_{iter}	209	311	178
V/V_0	32.85%	29.61%	29.42%
$t(s)$	9541	62137	6891

Compared with the initial design, the optimized design does alleviate the stress concentration substantially in Fig. 4.4. The stress concentration of topological structures optimized by the GCMMA algorithm is the most serious. The results show our algorithm can further reduce

(a) MMA, $\sigma_{\max} = 358GPa$, $V/V_0 =$ 32.85%

(b) GCMMA, $\sigma_{\max} = 358GPa$, $V/V_0 = 29.61\%$

(c) ADMM-MMA, $\sigma_{\max} = 358GPa$, $V/V_0 = 29.42\%$

(d) MMA, $N_{iter} = 209$

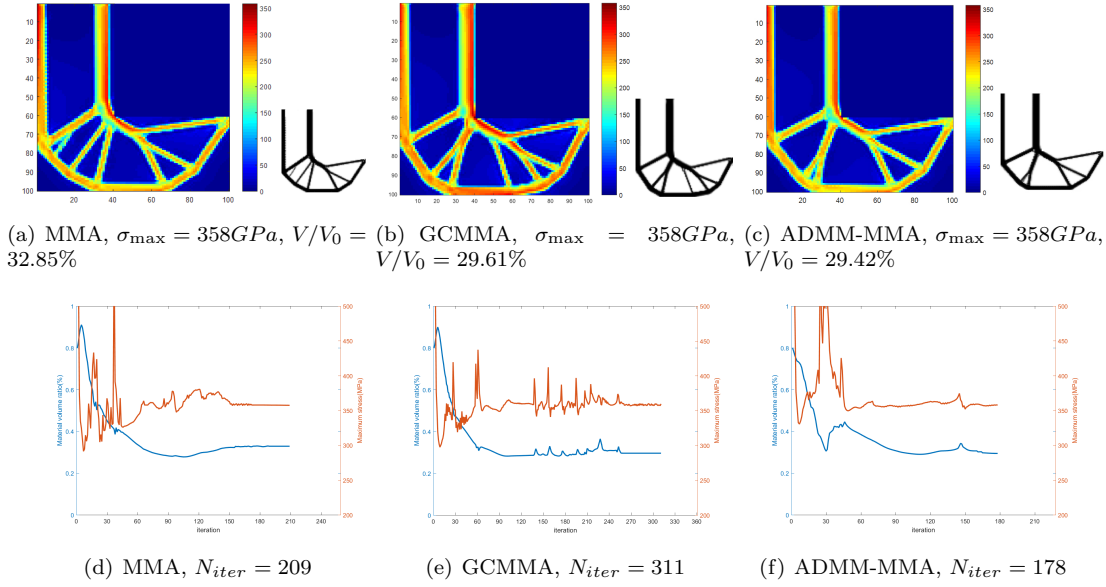(e) GCMMA, $N_{iter} = 311$

(f) ADMM-MMA, $N_{iter} = 178$

Fig. 4.4. Comparison results on L-shape examples with MMA, GCMMA and ADMM-MMA shows in the first row. Convergence curves(volume ratio and max von Mises stress) on the L-shape structure shows in the second row.

the volume ratio while avoiding stress concentration. We can find that our algorithm converges faster and is more stable than the other two algorithms. The curve oscillation produced by the GCMMA solver is the most obvious.

4.3. The rectangle domain design

In this subsection, the rectangle domains, that are, the Messerschmitt-Bolkow-Blohm (MBB) beam example and cantilever beam example, are adopted to test the numerical performance of a topology optimization approach, and demonstrate the stability of the presented approach. In MBB beam structure, we test two situations, that are, single external force (shown in Fig. 4.5(a)) and multiple external forces (shown in Fig. 4.5(b)). In the first situation, the left edge and bottom-right corner are fixed in the x direction and y direction, respectively. The downward force is acting in the top-left corner. In the second situation, we perform two external forces on the top boundary and fix the lower-left corner point and the lower-right corner point. As for the cantilever beam structure, the left edge is fixed in the x direction. The downward force is acting on the middle-left point (shown in Fig. 4.5(c)).
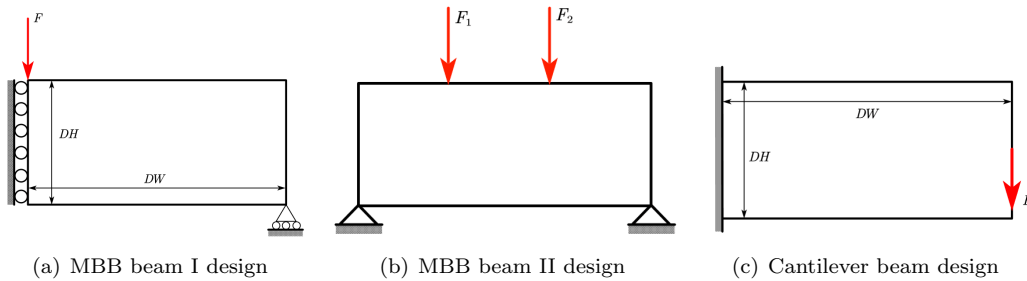

(a) MBB beam I design

(b) MBB beam II design

(c) Cantilever beam design

Fig. 4.5. Rectangle domain test examples.

(a) MMA, $N_{iter} = 172$ (b) GCMMA, $N_{iter} = 382$ (c) ADMM-MMA, $N_{iter} = 160$
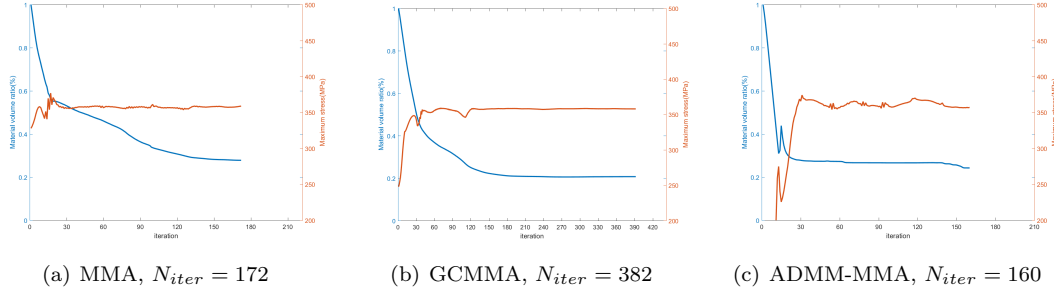
Fig. 4.6. The convergence curve of three algorithms on MBB beam I.

Table 4.4: Comparison results on rectangle domain examples among MMA, GCMMA and ADMM-MMA.

Examples	Factors	MMA	GCMMA	ADMM-MMA
MBB beam I	N_{iter}	172	382	160
	V/V_0	27.80%	20.73%	24.62%
	t(s)	9405	27704	8759
MBB beam II	N_{iter}	243	542	235
	V/V_0	35.62%	25.13%	28.65%
	t(s)	9300	19829	7941
Cantilever beam	N_{iter}	215	1000	189
	V/V_0	35.68%	37.36%	33.37%
	t(s)	8763	71506	8233

We summarize the factors N_{iter}, V/V_0 and $t(s)$ of three examples (MBB beam I, MBB beam II, Cantilever beam) in Table 4.4. The results are consistent with the previous two cases, that is, the convergence of ADMM-MMA is faster than MMA's and GCMMA's. In the three examples, our algorithm has the least number of iteration steps and optimization time. The number of iteration steps is 15 less than the MMA algorithm and 447 less than the GCMMA algorithm on average. The optimization time is 12.7% less than the MMA algorithm. At the same time, our final optimization result is better than MMA, equal to or even better than GCMMA.

The isogeometric topology optimization (ITO) results of three examples with different algorithms are shown in Fig. 4.7. Fig. 4.7(a)-(c) is the ITO results of MBB beam I. Fig. 4.7(b)-(d) is the ITO results of MBB beam II. Fig. 4.7(b)-(d) is the ITO results of the Cantilever beam. The first row represents the stress distribution, the second row represents the topology optimization structures. The color bar of stress distribution ranges from 0 GPa to 358 GPa. The color bar of topology structures ranges from 0 to 1. As can be seen from the figure, our algorithm optimization results are stable and similar to MMA results, while GCMMA optimization results are relatively not stable (see Fig. 4.7(h)). All three algorithms can effectively avoid the occurrence of stress concentration, and our algorithm performs best.See the white box in Fig. 4.7. In Fig. 4.6, our algorithm converges faster than the other two algorithms. In the case of tests in rectangular fields, the iterations are relatively stable. It should be noted that in the iteration process of the second example MBB beam II, the GCMMA algorithm converges slowly, and it reaches the maximum iteration step number $\max_{iter} = 1000$. And then, we stop the iteration and take the result of iteration 1000 for analysis.
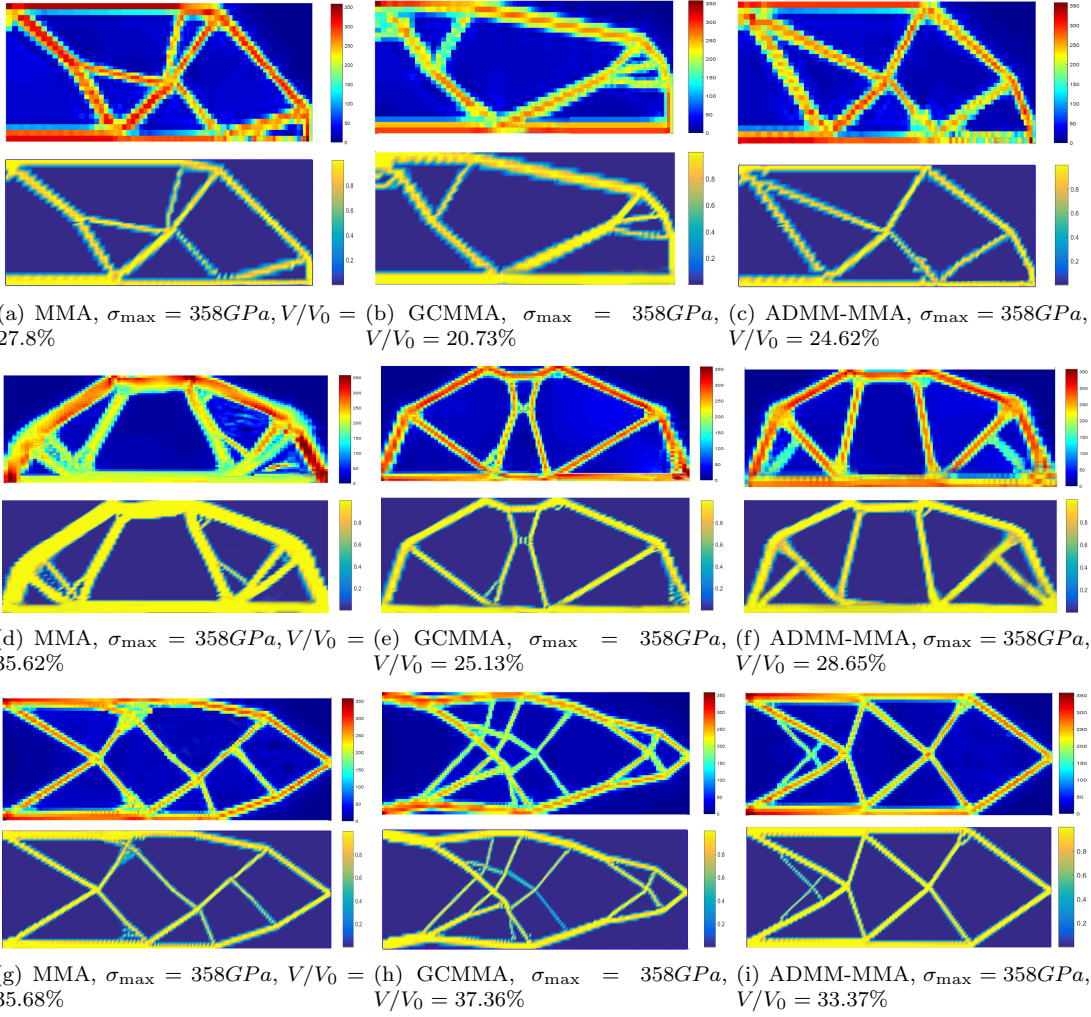
(a) MMA, $\sigma_{\max} = 358GPa, V/V_0 = 27.8\%$

(b) GCMMA, $\sigma_{\max} = 358GPa$, $V/V_0 = 20.73\%$

(c) ADMM-MMA, $\sigma_{\max} = 358GPa$, $V/V_0 = 24.62\%$

(d) MMA, $\sigma_{\max} = 358GPa, V/V_0 = 35.62\%$

(e) GCMMA, $\sigma_{\max} = 358GPa$, $V/V_0 = 25.13\%$

(f) ADMM-MMA, $\sigma_{\max} = 358GPa$, $V/V_0 = 28.65\%$

(g) MMA, $\sigma_{\max} = 358GPa, V/V_0 = 35.68\%$

(h) GCMMA, $\sigma_{\max} = 358GPa$, $V/V_0 = 37.36\%$

(i) ADMM-MMA, $\sigma_{\max} = 358GPa$, $V/V_0 = 33.37\%$

Fig. 4.7. Comparison results on rectangle domain with MMA, GCMMA and ADMM-MMA.

4.4. Discussioin

In this subsection, we have a discussion on four aspects. We first work on the parameters of the ADMM-MMA solver and illustrate the effectiveness of our algorithm. After that, we study the preponderance of IGA compared to FEA and show that our algorithm is still applicable for FEA. Finally, we research on the relationship between a number of design variables and optimization time and explain the challenge of 3D isogeometric topology optimization.

4.4.1. Discussion on ADMM solver

Firstly, we review the process of the ADMM optimizer. ADMM divides the original problem into two blocks. We optimize density ρ in the first block and stress σ in the second block. During the initial iteration, we expected density descending takes precedence over stress constraints. In subsequent iterations, that is, after the density has decreased to a certain extent, we expect the optimized structure to meet the stress constraint conditions, in other words, the stress constraint conditions have higher priority. Therefore, during the iteration, we need to update

Table 4.5: The data statistics on ADMM iteration steps and total steps, iteration time and the total time of the five examples.

Examples	Quarter annulus	L-shape design	MBB beam I	MBB beam II	Cantilever beam
N_{ADMM}	30	30	16	26	32
N_{tol}	143	178	160	235	189
N_{ADMM}/N_{tol}	20.98%	16.85%	10.00%	11.06%	16.93%
$t_{ADMM}(s)$	1584	1130	1131	447	1923
$t_{tol}(s)$	4856	6891	8759	7941	8233
t_{ADMM}/t_{tol}	32.62%	16.40%	12.91%	5.63%	23.36%
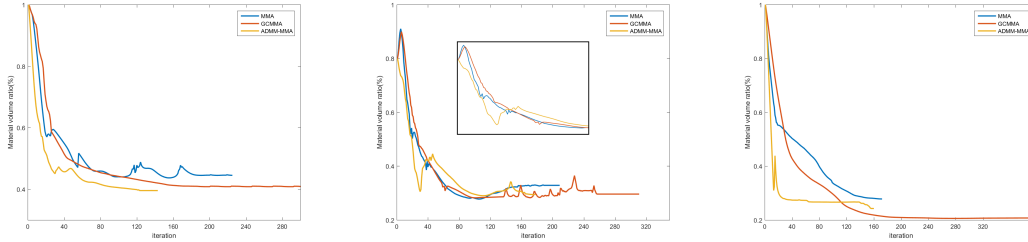
(a) Quarter annulus structure design   (b) L-shape design   (c) MBB beam I design

Fig. 4.8. Comparison of iterative curves for three algorithms (MMA, GCMMA and ADMM-MMA).

not only Lagrange multiplier λ, but also parameter μ. Beyond that, we need to define three maximum iterations during the iterations. They are the number of outer-iteration N_{outer}, the number of inner-iteration N_{inner}^1 of the first optimization block, and the number of inner-iteration N_{inner}^2 of the second optimization block. In this paper, we set $N_{outer} = 30$, $N_{inner}^1 = 5$ and $N_{inner}^2 = 20$. The condition for iteration termination is the value of the objective function produced by the ADMM iteration increases.

Secondly, we analyze the number of iteration steps and time-consuming of ADMM solver in Table 4.5. The second row to the fourth row of Table 4.5 shows a number of iteration steps. The average number of iteration steps of ADMM is 14.72% of the total number of iteration steps. The fifth row to the seventh row of Table 4.5 shows that the ADMM optimizer is time-consuming. ADMM time consumption accounts for 16.89% of the total optimization time.

Finally, for each example, the objective function optimization curves of the three algorithms are drawn in Fig. 4.4.1 so as to see the iterative process more clearly. As you can see from these figures, ADMM declines most rapidly during the initial iteration. In a later iteration, we adopted the MMA algorithm with the STM stability scheme. It can also achieve convergence results.

4.4.2. Applicability of FEA

IGA is a special finite element because the basis function is NURBS basis. Therefore, our algorithm is still applicable to FEA. It is worth noting that NURBS parameterization can provide exact geometry representation, that is, there is no approximation error for the geometric modeling at all levels of discretization. The comparisons of computational time using IGA and FEA are introduced in paper [31] in detail. The computational efficiency of IGA is higher under the same accuracy. Furthermore, paper [31] shows that IGA is more suitable for stress analysis. Since this paper focuses on IGA, we give the following example in order to illustrate the applicability of the algorithm on FEA.

(a) MMA   (b) GCMMA   (c) ADMM-MMA
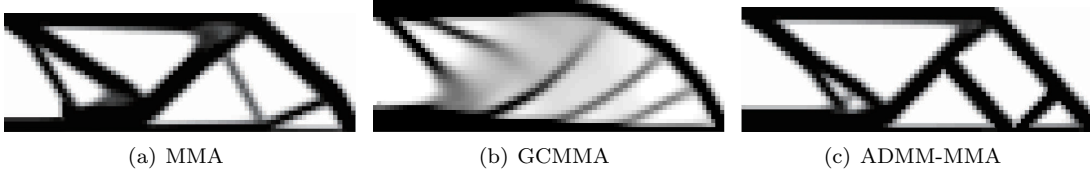
Fig. 4.9. Topology optimization of MMB beam I based on MMA, GCMMA, and ADMM-MMA.

Table 4.6: Comparison results on MBB beam I based on FEA by MMA, GCMMA and ADMM-MMA.

Methods	MMA	GCMMA	ADMM-MMA
N_{iter}	1542	10000	863
V/V_0	38.68%	32.15%	35.89%
$t(s)$	876	13310	758

Fig. 9 shows the optimized results tested on MBB beam I by MMA, GCMMA and ADMM-MMA. As can be seen from Table 4.6, the number of iterations is much higher than that of the iteration number based on IGA. Our algorithm has the least number of iteration steps. When the number of iteration steps of GCMMA reaches 10000, it still does not converge completely, but it has the lowest target function value. From the above, our algorithm still has advantages in optimization time and a number of iteration steps.

Fig. 4.10 shows the iterative process by three algorithms. It is consistent with the conclusion of topology optimization algorithm based on IGA. Our algorithm drops fast at first loops and has a good convergence.
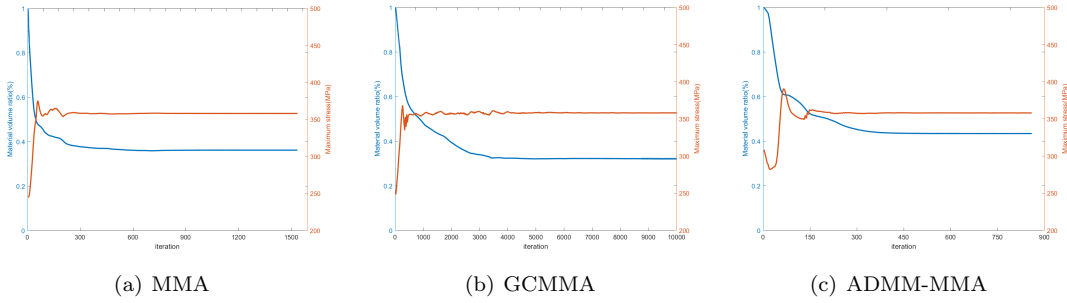

(a) MMA   (b) GCMMA   (c) ADMM-MMA

Fig. 4.10. Comparisons of iterative curves of three algorithms (MMA, GCMMA, ADMM-MMA).

4.4.3. Relationship between the number of design variables and optimization time

We calculate the relationship between the number of independent variables and iteration time to determine the possibility of generalization to 3D. We use N_{QA}, N_{RD}, N_L to represent number of variables, t_{QA}, t_{MBBI}, t_{MBBII}, t_{CB} and t_L to represent optimization time. We analyze the number of variables and optimization time in the test examples under different elements in Tables 4.7 and 4.8, respectively.

We take the number of variables as the horizontal coordinate(x) and the optimization time as the vertical coordinate(y) to establish the relationship between the number of variables and time and display it in Fig. 4.11. We use polynomial functions f_i (i=1,2,3,4,5) to fit each curve.

Table 4.7: The number of variables of five examples on a different number of elements.

N_{ele}	30×20	50×30	60×40	70×50	80×60	100×70	120×80
N_{QA}	704	1664	2604	3744	5084	7344	10004
N_{RD}	759	1749	2709	3869	5229	7519	10209
N_{ele}	30×30	40×40	50×50	60×60	70×70	80×80	100×100
N_L	1024	1764	2704	3844	5184	6724	10404

Table 4.8: The optimization time of five examples on a different number of elements.

N_{ele}	30×20	50×30	60×40	70×50	80×60	100×70	120×80
t_{QA}	194	837	1543	2476	3218	4856	6893
t_{MBBI}	379	1398	2812	3692	4783	5984	8759
t_{MBBII}	312	1876	2365	3292	4193	5494	7941
t_{CB}	420	1196	2175	3688	4988	6078	8333
N_{ele}	30×30	40×40	50×50	60×60	70×70	80×80	100×100
t_L	194.7854	473.1793	819.4591	1234.2001	2765.1942	4187.3762	6891.2561

An average fitting curve $\bar{f}$ is obtained by weighting.

$$\bar{f} = \frac{1}{5}(f_1 + f_2 + f_3 + f_4 + f_5) \tag{4.1}$$
$$= a \cdot x^2 + b \cdot x^1 + c,$$

where a $= 1.87e^{-5}$, b $= 0.94626$, c $= -472.08$. When the topology optimization problem rises to 3D, the degree of freedom is increased in the z-direction. Let's take $30 \times 20 \times 30$ on the rectangle domain as an example. The number of variables is approximate 21120. We plug it into Eq. 4.1. The results show that the approximate estimated optimization time is 27856 s. Therefore, it is still a challenge to raise the problem of topology optimization with stress constraints in 3D situations.
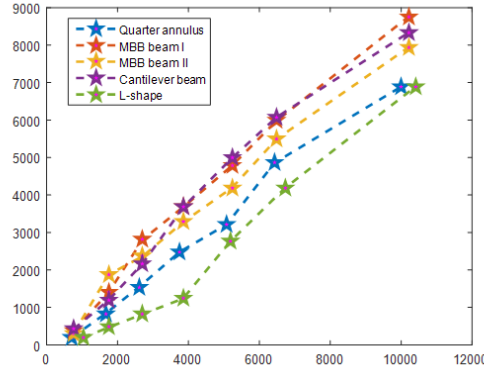

Fig. 4.11. The trend of several design variables and optimization time.

5. Conclusion and Future Work

This paper presents a hybrid optimization method to solve the problem of isogeometric topology optimization based on stress-limited. We first use ADMM to get a feasible point be-

cause of its fast convergence at the beginning loops; after that, MMA is adopted to get final optimal results. To further verify the effectiveness of the proposed algorithm, we compare our algorithm with the classical algorithm MMA and GCMMA. GCMMA proved to be globally convergent. But in the practical test, it convergences slowly due to the iterative oscillation. The MMA algorithm is iteratively stable. So we use ADMM to accelerate it in the initial stage further. Because topology optimization with stress constraints is highly nonlinear, iterative oscillation cannot be avoided strictly in the optimization process. Despite this, several benchmark numerical examples are presented to demonstrate the proposed approach's robustness, stability, and effectiveness.

Although our algorithm has better efficiency in numerical examples, it still suffers from some deficiencies. Since topology optimization with stress constraints is a highly nonlinear problem, it is difficult for an algorithm that avoids iterative oscillations completely. Due to the high complexity of this problem, topology optimization with stress constraints in 3D still faces challenges such as inefficiency calculation, slow convergence, and so on. Parameterization of 3D models will also be an important but complex problem. In the following work, we will study the acceleration algorithm of 3D topology optimization and try to find a better algorithm.

References

[1] F. Zanettin, Topology Optimization - Wikipedia, 2000.

[2] M.P. Bendsøe and N. Kikuchi, Generating optimal topologies in structural design using a homogenization method, *Computer Methods in Applied Mechanics and Engineering*, **71**:2 (1988), 197–224.

[3] O. Sigmund, A 99 line topology optimization code written in matlab, *Structural and Multidisciplinary Optimization*, **21**:2 (2001), 120–127.

[4] E. Andreassen, A. Clausen, M. Schevenels, B.S. Lazarov and O. Sigmund, Efficient topology optimization in matlab using 88 lines of code, *Structural and Multidisciplinary Optimization*, **43**:1 (2011), 1–16.

[5] G. Allaire, F. Jouve and A.M. Toader, Structural optimization using sensitivity analysis and a level-set method, *Journal of Computational Physics*, **194**:1 (2004), 363–393.

[6] W. Zhang, J. Yuan, J. Zhang and X. Guo, A new topology optimization approach based on moving morphable components (mmc) and the ersatz material model, *Structural and Multidisciplinary Optimization*, **53**:6 (2016), 1243–1260.

[7] X. Guo, W. Zhang, J. Zhang and J. Yuan, Explicit structural topology optimization based on moving morphable components (mmc) with curved skeletons, *Computer Methods in Applied Mechanics and Engineering*, **310** (2016), 711–748.

[8] W. Zhang, J. Chen, X. Zhu, J. Zhou, D. Xue, X. Lei and X. Guo, Explicit three dimensional topology optimization via moving morphable void (mmv) approach, *Computer Methods in Applied Mechanics and Engineering*, **322** (2017), 590–614.

[9] W. Zhang, D. Li, J. Zhou, Z. Du, B. Li and X. Guo, A moving morphable void (mmv)-based explicit approach for topology optimization considering stress constraints, *Computer Methods in Applied Mechanics and Engineering*, **334** (2018), 381–413.

[10] T.J. Hughes, J.A. Cottrell and Y. Bazilevs, Isogeometric analysis: Cad, finite elements, nurbs, exact geometry and mesh refinement, *Computer Methods in Applied Mechanics and Engineering*, **194**:39–41 (2005), 4135–4195.

[11] Y.D. Seo, H.J. Kim and S.K. Youn, Isogeometric topology optimization using trimmed spline surfaces, *Computer Methods in Applied Mechanics and Engineering*, **199**:49-52 (2010), 3270–3296.

[12] A.V. Kumar and A. Parthasarathy, Topology optimization using b-spline finite elements, *Structural and Multidisciplinary Optimization*, **44**:4 (2011), 471.

[13] B. Hassani, M. Khanzadi and S.M. Tavakkoli, An isogeometrical approach to structural topology optimization by optimality criteria, *Structural and Multidisciplinary Optimization*, **45**:2 (2012), 223–233.

[14] X. Qian, Topology optimization in b-spline space, *Computer Methods in Applied Mechanics and Engineering*, **265** (2013), 15–35.

[15] H.Y. Lin, M. Rayasam and G. Subbarayan, Isocomp: Unified geometric and material composition for optimal topology design, *Structural and Multidisciplinary Optimization*, **51**:3 (2015), 687–703.

[16] Y. Wang, H. Xu and D. Pasini, Multiscale isogeometric topology optimization for lattice materials, *Computer Methods in Applied Mechanics and Engineering*, **316** (2017), 568–585.

[17] R. Yang and C. Chen, Stress-based topology optimization, *Structural optimization*, **12**:2–3 (1996), 98–105.

[18] M.P. Bendsoe and O. Sigmund, Topology Optimization: Theory, Methods, and Applications, Springer Science & Business Media, 2003.

[19] M.P. Bendsøe, Topology Optimization, Springer, 2009.P

[20] K. Lee, K. Ahn and J. Yoo, A novel p-norm correction method for lightweight topology optimization under maximum stress constraints, *Computers & Structures*, **171** (2016), 18–30.

[21] Y. Luo, M.Y. Wang and Z. Kang, An enhanced aggregation method for topology optimization with local stress constraints, *Computer Methods in Applied Mechanics and Engineering*, **254** (2013), 31–41.

[22] C. Le, J. Norato, T. Bruns, C. Ha and D. Tortorelli, Stress-based topology optimization for continua, *Structural and Multidisciplinary Optimization*, **41**:4 (2010), 605–620.

[23] S. Amstutz and A.A. Novotny, Topological optimization of structures subject to von mises stress constraints, *Structural and Multidisciplinary Optimization*, **41**:3 (2010), 407–420.

[24] M.Y. Wang and L. Li, Shape equilibrium constraint: a strategy for stress-constrained structural topology optimization, *Structural and Multidisciplinary Optimization*, **47**:3 (2013), 335–352.

[25] W.S. Zhang, X. Guo, M.Y. Wang and P. Wei, Optimal topology design of continuum structures with stress concentration alleviation via level set method, *International Journal for Numerical Methods in Engineering*,P **93**:9 (2013), 942–959.

[26] E. Holmberg, B. Torstenfelt and A. Klarbring, Stress constrained topology optimization, *Structural and Multidisciplinary Optimization*, **48**:1 (2013), 33–47.

[27] A. Francavilla, C.V. Ramakrishnan and O.C. Zienkiewicz, Optimization of shape to minimize stress concentration, *Journal of Strain Analysis*, **10**:2 (1975), 63–70.

[28] W.D. Pilkey and D.F. Pilkey, Peterson's stress concentration factors, John Wiley & Sons, 2008.

[29] G. Cheng and X. Guo, ε-relaxed approach in structural topology optimization, *Structural Optimization*, **13**:4 (1997), 258–266.

[30] M. Bruggi, On an alternative approach to stress constraints relaxation in topology optimization, *Structural and Multidisciplinary Optimization*, **36**:2 (2008), 125–141.

[31] H. Liu, D. Yang, P. Hao and X. Zhu, Isogeometric analysis based topology optimization design with global stress constraint, *Computer Methods in Applied Mechanics and Engineering*, **342** (2018), 625–652.

[32] X.P. Yunkang Sui, Modeling, Solving and Application for Topology Optimization of Continuum Sturctures ICM Method Based on Step Function, Tsinghua University Press, 2018.

[33] P. Tanskanen, The evolutionary structural optimization method: theoretical aspects, *Computer Methods in Applied Mechanics and Engineering*, **191**:47-48 (2002), 5485–5498.

[34] P.T. Boggs and J.W. Tolle, Sequential quadratic programming, *Acta Numerica*, **4** (1995), 1–51.

[35] A. Forsgren and P.E. Gill, Primal-dual interior methods for nonconvex nonlinear programming, *SIAM Journal on Optimization*, **8**:4 (1998), 1132–1152.

[36] K. Svanberg, The method of moving asymptotesa new method for structural optimization, *International Journal for Numerical Methods in Engineering*, **24**:2 (1987), 359–373.

[37] K. Svanberg, A class of globally convergent optimization methods based on conservative convex

separable approximations, *SIAM Journal on Optimization*, **12**:2 (2002), 555–573.

[38] S. Rojas-Labanda and M. Stolpe, Benchmarking optimization solvers for structural topology optimization, *Structural and Multidisciplinary Optimization*, **52**:3 (2015), 527–547.

[39] H. Adeli and N.T. Cheng, Augmented lagrangian genetic algorithm for structural optimization, *Journal of Aerospace Engineering*, **7**:1 (1994), 104–118.

[40] O. Hasançebi and F. Erbatur, Layout optimisation of trusses using simulated annealing, *Advances in Engineering Software*, **33**:7–10 (2002), 681–696.

[41] R. Poli, J. Kennedy and T. Blackwell, Particle swarm optimization, *Swarm Intelligence*, **1**:1 (2007), 33–57.

[42] H.A. Eschenauer and N. Olhoff, Topology optimization of continuum structures: a review, *Applied Mechanics Reviews*, **54**:4 (2001), 331–390.